Effect of the phase transition of $LiSn_2(PO_4)_3$ on the Li^+ ion conduction in $LiSn_2(PO_4)_3$ - Teflon composites

1997 J. Phys.: Condens. Matter 9 4119

(http://iopscience.iop.org/0953-8984/9/20/011)

J. Phys.: Condens. Matter **9** (1997) 4119–4128. Printed in the UK PII: S0953-8984(97)81328-8

Effect of the phase transition of $LiSn_2(PO_4)_3$ on the Li^+ ion conduction in $LiSn_2(PO_4)_3$–Teflon composites

Ana Martinez-Juarez†, Ricardo Jimenez†, Pedro Duran-Martin†, Joaquin Ibañez‡ and Jose M Rojo†§

† Instituto Ciencia de Materiales de Madrid, CSIC, Cantoblanco, 28049-Madrid, Spain

‡ Centro Nacional de Investigaciones Metalurgicas, CSIC, Avda Gregorio del Amo 8, 28049-Madrid, Spain

Received 27 January 1997, in final form 17 March 1997

Abstract. A composite $LiSn_2(PO_4)_3$–25% vol Teflon was prepared to prevent breakages in powder pellets due to the phase transition of $LiSn_2(PO_4)_3$ and, thus, to study the effect of the phase transition on Li^+ conduction. The composite microstructure, as followed by scanning electron microscopy, shows aggregated $LiSn_2(PO_4)_3$ particles surrounded by Teflon regions which operate as a skeleton. The imaginary part of the electric modulus shows two peaks at high and low frequency which are ascribed to grain-interior and grain-boundary response, respectively. In the two phases the ionic conductivity inside the grains is about three orders of magnitude larger than that found for the grain boundary. The phase transition affects the activation energy in different ways. It decreases for the grain-interior response from 0.68 eV for the low-temperature phase to 0.34 eV for the high-temperature phase, while it increases from 0.45 to 0.56 eV for the Li^+ movement through the grain boundaries. An anomalous increase in activation energy for the grain-interior response in the high-temperature phase before it is transformed into the low-temperature phase has been found.

1. Introduction

Materials with NASICON-type structure are, in general, good ion conductors due to the presence of channels in which alkali ions can move easily [1, 2]. $LiSn_2(PO_4)_3$ belongs to this kind of materials; its framework is built up of SnO_6 octahedra and PO_4 tetrahedra sharing corners. The Li^+ ions can occupy two crystallographic sites which are separated by triangular bottlenecks of oxygens. One site (M2) is placed at the bend of each channel, and the other (M1) at the intersection of three channels [3–6].

On the other hand, $LiSn_2(PO_4)_3$ exhibits a reversible first-order phase transition with a hysteresis cycle in temperature [7, 8]. The symmetry changes from monoclinic Cc, for the low-temperature phase, to rhombohedral $R\bar{3}c$, for the high-temperature phase, the last symmetry being the usual one found for NASICON-type materials. Both phases coexist in the temperature range 100–140 °C and 60–20 °C during the heating and cooling run, respectively [8]. The phase transition yields a change in the lattice volume leading to breakages in pressed powder pellets and preventing electrical study during the phase transition. To overcome this we have prepared a composite in which Teflon was used as a binder to improve handling. To the best of our knowledge, composites of ion-conducting particles dispersed in Teflon have not yet been studied, although composites of metal or black

§ Author to whom correspondance should be addressed.

0953-8984/97/204119+10$19.50

carbon particles dispersed in Teflon and other polymeric matrices have been extensively [9–15].

In this work we have prepared pellets of a composite in which the amount of Teflon (10% by weight) was minimum to ensure good contacts among $LiSn_2(PO_4)_3$ particles. We have studied this composite in order to understand the effect of the phase transition of $LiSn_2(PO_4)_3$ on the a.c. electrical properties due to Li^+ conduction inside the $LiSn_2(PO_4)_3$ particles and through the boundaries of neighbouring particles.

2. Experimental procedure

$LiSn_2(PO_4)_3$ was prepared according to the formation process described elsewhere [16]. Teflon was chosen as a binder because: (i) the significant low conductivity, $\sigma \approx 10^{-19}$ ohm^{-1} cm^{-1} at room temperature; (ii) the low and practically constant permittivity ($\varepsilon_r' = 2.1$) over a wide frequency range (60–10^6 Hz); and (iii) the relatively high thermal stability, $T_g = 270\,^{\circ}$C, which allows heating of the composite to this temperature. The composite (10% by weight or 25% by volume in Teflon) was prepared by mixing and grinding in an agate mortar the powder $LiSn_2(PO_4)_3$ sample with a commercial Teflon. Then pellets of approximately 12 mm diameter and 1 mm thickness were obtained by cold pressing the composite at 400 MPa for 10 min. The pellets were annealed at 230 °C, i.e. 40 °C below the T_g-Teflon temperature, for 2 h.

Platinum electrodes were deposited on the two faces of the pellets by sputtering. Impedance measurements were carried out in the frequency range 0.1–10^5 Hz on a 1174 Solartron frequency response analyser coupled to a 1286 Solartron electrochemical interface. Impedance measurements were also carried out in the frequency range 500–10^7 Hz by using a 4194A Hewlet Packard. In both cases the data were obtained while the pellet was at a steady temperature. The temperature range was 60–220 ° C. The pellets were subjected to heating and cooling runs under nitrogen flow.

The microstructural characterization of the material was carried out by optical microscopy (OM), and scanning electron microscopy (SEM) coupled to an energy dispersive spectrometer (EDS). Conventional metallographic procedures included mounting in a resin and polishing, both in transverse and longitudinal sections of the pellets, were used. To avoid charging effects in SEM observations the samples were coated with a carbon film. Particle size measurements were performed with an image analyser from digitalized SEM micrographs.

3. Results and discussion

The Teflon powder used as examined by optical microscopy is shown in figure 1. The particles show a granular texture with sizes in the range 300–800 μm.

A pellet of the $LiSn_2(PO_4)_3$-Teflon composite was cut in the direction normal to the pellet surface. The scanning electron micrographs corresponding to this view are shown in figures 2(*a*) and 2(*b*); the first figure shows the overall section of the pellet, and the last one a magnified picture of the region marked in figure 2(*a*). From electron probe microanalysis data the white particles were ascribed to $LiSn_2(PO_4)_3$ and the black areas to Teflon. The texture of the Teflon regions is quite different from that of the starting particles; the elongated shape points to a deformation of the starting particles in a direction which is normal to that of the force applied during the pellet compactation (see arrows in figure 2(*a*)). This fact has been also observed in composites formed of metal particles and other polymeric matrices

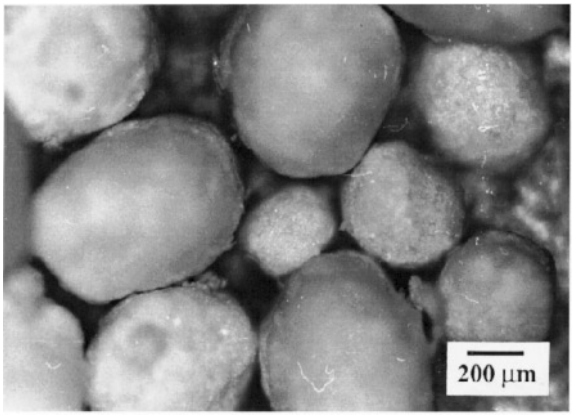

Figure 1. Optical micrograph of starting Teflon powder.

[17]. In our case, Teflon does not surround every $LiSn_2(PO_4)_3$ particle; the $LiSn_2(PO_4)_3$ particles are aggregated in regions which are partially surrounded by Teflon. The Teflon regions are interconnected, and this fact seems to improve the mechanical properties of the pellet. The size distribution of the $LiSn_2(PO_4)_3$ particles is shown in figure 3. The average size and standard deviation are 5.7 and 4.9 μm, respectively.

The impedance plots (imaginary against real part) recorded at different temperatures are shown in figure 4. A depressed arc and an inclined spike are observed. The spike is due to the blocking effect of Li^+ ions at the electrodes [18] while the arc gives information about the dielectric response of the composite. Taking into account the fact that the conducting phase is formed by aggregation of particles or grains, a differentiation of the grain-interior and grain-boundary response should be expected. However, only one arc is observed suggesting that both responses are overlapped.

In order to separate the two responses, as well as to estimate their contribution to the overall conductivity of the pellet, the real part of the conductivity, $\sigma'(\omega)$, related to the impedance through the expression

$$\sigma'(\omega) = Z'(\omega)/(Z'(\omega)^2 + Z''(\omega)^2)$$

is shown in figure 5 as a function of angular frequency for different temperatures. Two plateaux associated with d.c. conductivities are observed: one in the low-frequency region and the other in the high-frequency region, corresponding to the grain-boundary and grain-interior response, respectively. The significant difference of the two d.c. values accounts for the lack of resolution found in the impedance plots (figure 4). Two dispersive regimes of the form ω^n, at low and high frequencies, are also observed. At low temperatures (see the plot at 70 °C) the experimental data are well fitted to the expression

$$1/\sigma' = 1/\sigma'_{gb} + 1/\sigma'_{gi}$$

where σ', σ'_{gb} and σ'_{gi} are the overall, grain-boundary, and grain-interior conductivity, respectively. The expression used for σ'_{gb} and σ'_{gi} is of the form [19] $\sigma_{dc} + A\omega^n$. However, at intermediate and high temperatures (see the plot at 130 °C), i.e. when the grain-boundary response is well defined, we need two expressions for this response, σ'_{gb1} and σ'_{gb2} , in order to improve the fitting. In these cases the expression used was

$$1/\sigma' = 1/\sigma'_{gb1} + 1/\sigma'_{gb2} + 1/\sigma'_{gi}$$

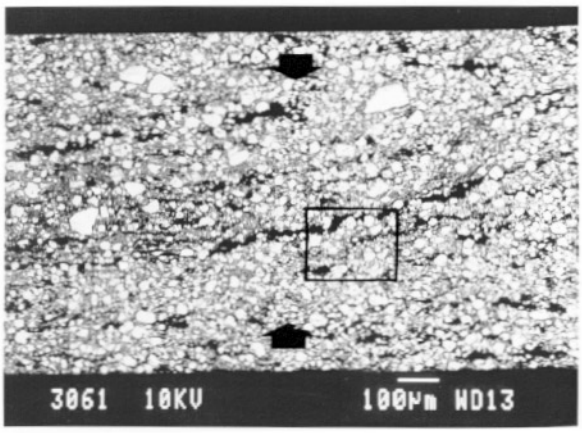

(*a*)

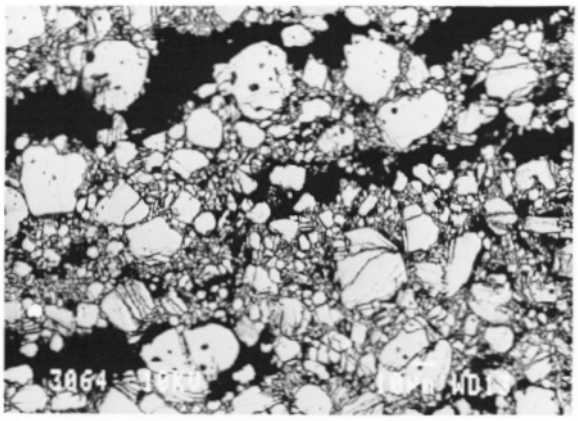

(*b*)

Figure 2. Backscattered electron images (BEI) of the pellet cross section. (*a*) The general view of the overall cross section, arrows indicate the compression stress direction during compactation, and (*b*) the magnified region marked in (*a*).

where for every conductivity we adopted the form $\sigma_{dc} + A\omega^n$ already mentioned. The study of this point is out of the scope of this paper; we only use the fitting to determine the overall and grain-interior d.c. conductivities. The significant difference of these conductivities, about three orders of magnitude, shows clearly that the overall conductivity is dominated by that for the grain boundary. The values of n were found to be in the range 0.85–0.95 for the grain-interior response and close to 1 for the grain-boundary response. The A parameter showed values of 10^{-13}–10^{-12} (ohm cm)$^{-1}$ s^n for both responses in the temperature range analysed.

The complex electric modulus, $M^*(\omega) = j\omega Z^*(\omega) = j\omega/\sigma^*(\omega)$, is widely used in glasses and ceramic materials because it gives information about the grain-interior response and is not usually affected by blocking phenomena, i.e. grain-boundary and electrode effects [20–22]. In fact $M^* \propto 1/C$, C being the capacitance which is of the order of magnitude of pF, nF, and μF for the grain-interior, grain-boundary, and electrode, respectively, in sintered ceramic materials [23]. The imaginary part (M'') as a function of frequency

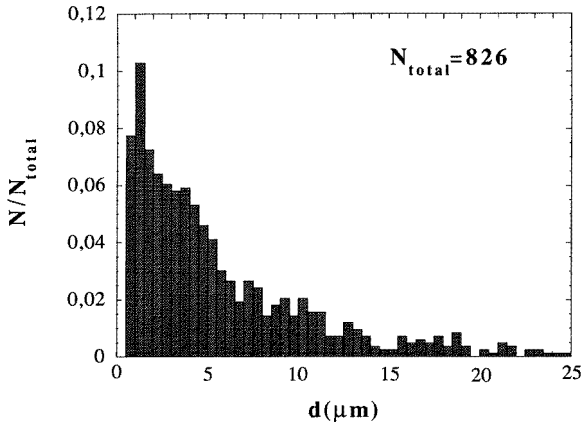

Figure 3. A size distribution histogram of $LiSn_2(PO_4)_3$ particles. The equivalent circle diameter (d) is the diameter of the circle having the same surface area as the particle examined.

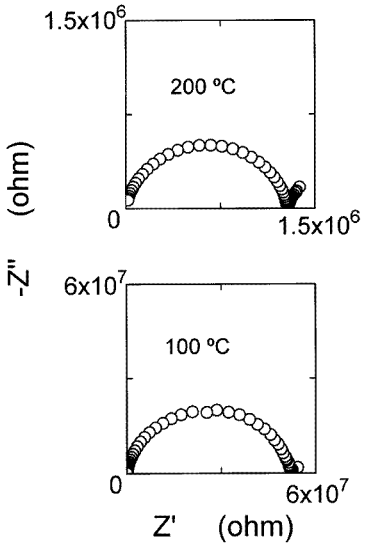

Figure 4. Impedance plots (imaginary against real part) obtained at two temperatures.

normally shows a peak associated with the grain-interior response from which the relaxation time $\tau = 1/f_{max}$, where f_{max} is the frequency at the maximum of the peak, can be obtained [24–26]. In contrast to this our M'' against frequency plot shows two peaks (figure 6). Their position shifts towards high frequency with rising temperature. According to the results of the real conductivity the low- and high-frequency M'' peaks are ascribed to the grain-boundary and grain-interior response, respectively. The height of the low-frequency M'' peak is approximately half that of the other peak indicating that the capacitance associated with the grain-boundary response is double that associated with the grain-interior one. This small difference contrasts again with the difference found for sintered ceramic materials as already mentioned.

The temperature dependence of the d.c. conductivity for the grain interior and overall is

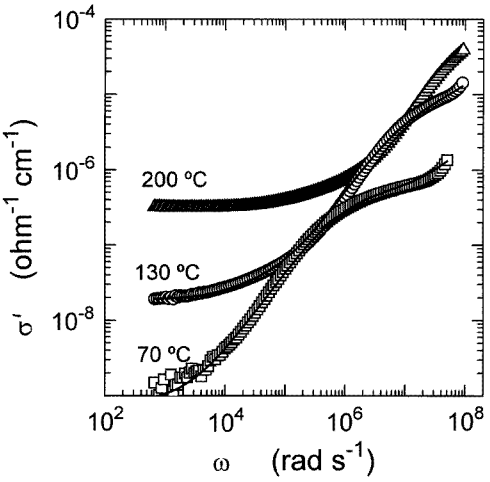

Figure 5. The real part of the conductivity against angular frequency at different temperatures. The experimental data recorded at 70 and 130 °C are fitted to the expressions $1/\sigma' = 1/\sigma'_{gb} + 1/\sigma'_{gi}$ and $1/\sigma' = 1/\sigma'_{gb1} + 1/\sigma'_{gb2} + 1/\sigma'_{gi}$, respectively. σ'_{gi} is the grain-interior conductivity, and σ'_{gb}, σ'_{gb1}, and σ'_{gb2} are grain-boundary conductivities as described in the text. In all cases for the conductivity we adopted the form $\sigma_{dc} + A\omega^n$.

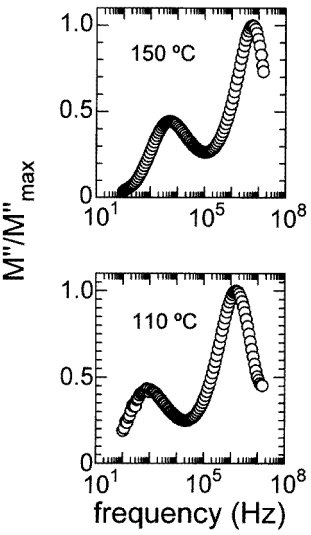

Figure 6. The normalized imaginary part of the electric modulus against frequency at the indicated temperatures.

shown (figure 7(*a*)) in an Arrhenius plot. The grain-interior data are represented by circles, and the overall data by triangles. The temperature dependence of the frequency measured at the maxima of the two M'' peaks is also shown in an Arrhenius plot (figure 7(*b*)). Squares correspond to the low-frequency peak and circles to the high-frequency one. In the two kinds of plots the data obtained in the heating and cooling runs are represented by open and

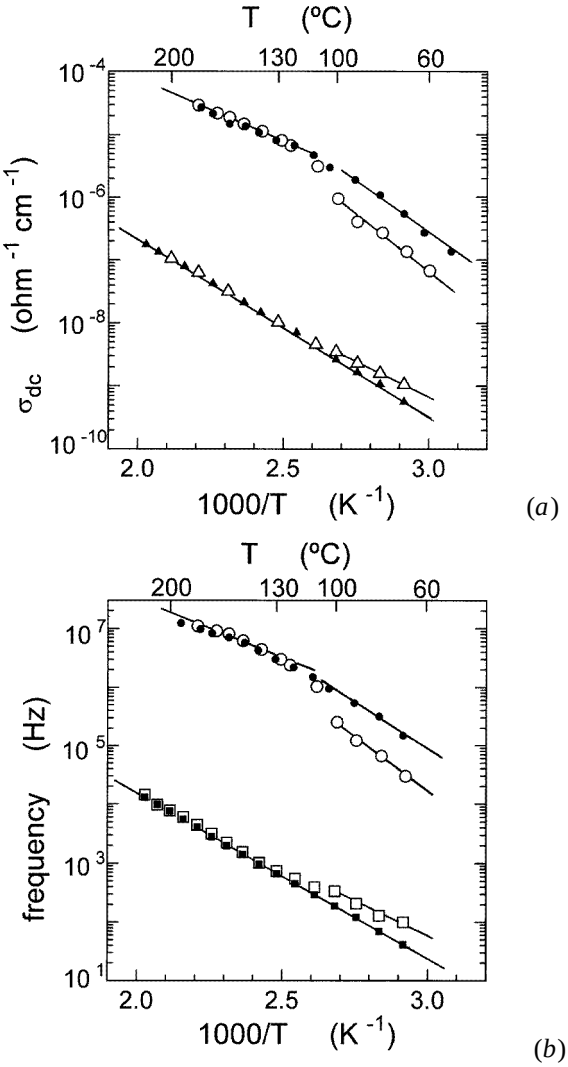

Figure 7. (*a*) d.c. conductivity against $1000/T$. Circles and triangles correspond to the grain-interior and overall conductivity, respectively. (*b*) Frequency at the maxima of the two M'' peaks against $1000/T$. Circles and squares correspond to the high-frequency and low-frequency M'' peaks, respectively. In both kinds of plots the data represented by open symbols refer to the heating run, and those by closed symbols to the cooling run. The full lines are the best fits to the expressions $\sigma = \sigma_0 \exp(-E_\sigma/KT)$, and $f = f_0 \exp(-E_f/KT)$.

closed symbols, respectively. The frequency data have been fitted to the expression

$$f = f_0 \exp(-E_f/KT)$$

and the d.c. conductivity data to

$$\sigma = \sigma_0 \exp(-E_\sigma/KT)$$

where f_0 and σ_0 are pre-exponential factors, E_f and E_σ are activation energies, and K is the Boltzmann constant. The fitting values are outlined in table 1. It is observed that: (i) the activation energies obtained for the high-frequency M'' peak coincide with

the values obtained for the grain-interior d.c. conductivity, and (ii) the activation energies obtained for the low-frequency M'' peak coincide with those obtained for the overall d.c. conductivity which is dominated by the grain-boundary response. Both facts support again the assignment of the low- and high-frequency M'' peak to grain-boundary and grain-interior response, respectively.

Table 1. Activation energies (E_f and E_σ) and pre-exponential factors (f_0 and σ_0) for the Arrhenius plots of figure 7.

Run	T (°C)	f_0 (Hz)	E_f (eV)	σ_0 (ohm^{-1} cm^{-1})	E_σ (eV)
Grain interior					
Heating	60–100	$8 \pm 6 \times 10^{14}$	0.71 ± 0.03	$1.0 \pm 0.4 \times 10^{4}$	0.68 ± 0.02
	130–200	$4 \pm 2 \times 10^{10}$	0.33 ± 0.01	1.4 ± 0.6	0.34 ± 0.01
Cooling	200–130	$4 \pm 2 \times 10^{10}$	0.33 ± 0.01	1.4 ± 0.6	0.34 ± 0.01
	100–60	$6 \pm 2 \times 10^{14}$	0.66 ± 0.02	$1.2 \pm 0.4 \times 10^{4}$	0.64 ± 0.02
Grain boundary/overall					
Heating	60–100	$4 \pm 2 \times 10^{8}$	0.45 ± 0.02	$5.8 \pm 0.6 \times 10^{-3}$	0.46 ± 0.02
	130–200	$8.0 \pm 0.5 \times 10^{9}$	0.56 ± 0.01	$9.2 \pm 0.7 \times 10^{-2}$	0.56 ± 0.01
Cooling	200–60	$8.0 \pm 0.5 \times 10^{9}$	0.56 ± 0.01	$9.2 \pm 0.7 \times 10^{-2}$	0.56 ± 0.01

In the heating run, the frequency and conductivity plots for the grain interior (open circles) and grain boundary (open squares and triangles) show two regimes: one below 100 °C and the other above 130 °C. Below 100 °C the low-temperature phase of $LiSn_2(PO_4)_3$ exhibits a monoclinic Cc symmetry, but the symmetry changes to rhombohedral $R\bar{3}c$ above 130 °C [8]. Then, we ascribe the two regimes observed to the two phases. The departure from the Arrhenius behaviour between 100 and 130 °C is due to the coexistence of both phases according to the x-ray diffraction and NMR data previously reported [8]. The activation energy for the grain-interior response, deduced from the frequency and d.c. conductivity data, is 0.68 eV for the low-temperature phase and 0.34 eV for the high-temperature phase. The activation energy for the grain-boundary response, also deduced from the two plots, is 0.45 eV for the low-temperature phase and 0.56 eV for the high-temperature phase. Then, the phase transition affects the movement of Li^+ ions inside the grains and through the grain boundaries in a different way. According to the model generally accepted for NASICON materials in which Li^+ ions are moving along the channels by jumping between M1 and M2 sites, the decrease in activation energy means that the jump becomes easier, probably due to a change in the bottleneck between the two sites. In contrast, the jump through the grain boundary is hindered suggesting a worsening of the contacts among particles.

When the composite is cooled in the range 200–60 °C a different behaviour for the grain-interior and grain-boundary response is observed. The grain-boundary response (closed squares and triangles) shows only one regime which coincides with that found for the high-temperature phase in the heating run. It agrees with the presence of this phase in the mentioned temperature range as deduced from x-ray diffraction and NMR data. Below 60 °C both phases coexist, although the high-temperature phase is progressively transformed into the low-temperature phase, and at 10 °C the low-temperature phase is obtained as a pure phase [8]. However, experimental limitations prevented us from performing measurements below 60 °C.

The grain-interior response (closed circles) in the cooling run between 200 and 130 °C shows the same linear dependences in the two plots as those found for the high-temperature

phase in the heating run. These results are consistent with the presence of the high-temperature phase in the range 200–130 °C. However, below 130 °C another regime of higher activation energy (0.65 eV) whose value is close to that found for the low-temperature phase is observed. It indicates that, in spite of the fact that the phase is still the high-temperature one, the movement of Li^+ ions along the channels is hindered. This suggests to us a modification of the bottleneck between the M1 and M2 sites, probably due to some strain of the framework. In any case, this behaviour precedes the phase transition in the cooling run, and to the best of our knowledge it is reported for the first time.

Once the low-temperature phase is obtained as a pure phase at 10 °C, the experimental data obtained in the first heating–cooling cycle are reproduced in a new cycle, in agreement with the reversible character of the phase transition [8].

4. Conclusions

An ion conductor composite formed of NASICON particles and Teflon has been prepared. The grain-interior and grain-boundary response are overlapped in the impedance plots but they can be distinguished in the real conductivity against frequency and imaginary modulus against frequency plots. The grain-boundary d.c. conductivity is about three orders of magnitude lower than that for the grain interior while the grain-boundary capacitance is only double that for the grain interior.

The phase transition is reversible and shows a hysteresis cycle in temperature for the grain-interior and grain-boundary response. The value of the activation energy associated with the two responses changes in an opposite way with the phase transition.

Acknowledgment

Financial support by CICYT (project MAT95-0899) is gratefully acknowledged.

References

[1] Goodenough J B, Hong H Y-P and Kafalas J A 1976 *Mater. Res. Bull.* **11** 203
[2] Hagman L and Kierkegaard P 1968 *Acta Chem. Scand.* **22** 1822
[3] Petit D, Colomban Ph, Collin G and Boilot J P 1986 *Mater. Res. Bull.* **21** 365
[4] Alami M, Brochou R, Soubeyroux J L, Gravereau P, Le Flem G and Hagenmuller P 1991 *J. Solid State Chem.* **90** 185
[5] Kohler H and Schulz H 1986 *Mater. Res. Bull.* **21** 23
[6] Paris M A, Martinez-Juarez A, Rojo J M and Sanz J 1996 *J. Phys.: Condens. Matter* **8** 5355
[7] Angenault J, Couturier J C, Souron J P, Siliqi D and Quarton M 1992 *J. Mater. Sci. Lett.* **11** 1705
[8] Martinez-Juarez A, Rojo J M, Iglesias J E and Sanz J 1995 *Chem. Mater.* **7** 1857
[9] Aharoni S M 1972 *J. Appl. Phys.* **43–5** 2463
[10] Fitzpatrick J P, Malt R B and Spaepen F 1974 *Phys. Lett.* **47A** 207
[11] Song Y, Noh T W, Lee S I and Gaines J R 1984 *Phys. Rev.* B **33–2** 904
[12] Pierse C, Deltour R, Perenboom J A A J and M Van Bentum P J 1990 *Phys. Rev.* B **42–6** 3380
[13] McLachlan D S, Blaszkiewitz M and Newnham R E 1990 *J. Am. Ceram. Soc.* **73–8** 2187
[14] Ruschau G R and Newham R E 1992 *J. Comp. Mat.* **26–18** 2727
[15] Celzard A, Furdin G, Mareche J F, McRae E, Dufort M and Deleuze C 1994 *Solid State Commun.* **92-5** 377
[16] Martinez A, Rojo J M, Iglesias J E, Sanz J and Rojas R M 1994 *Chem. Mater.* **6** 1790
[17] Malliaris A and Turner D T 1971 *J. Appl. Phys.* **42–2** 614
[18] Macdonald J R 1987 *Impedance Spectroscopy, Emphasizing Solid Materials and Systems* (New York: Wiley)
[19] Jonscher A K 1983 *Dielectric Relaxation in Solids* (London: Chelsea Dielectric)
[20] Macedo P B, Moynihan C T and Bose R 1972 *Phys. Chem. Glasses* **13** 171
[21] Hodge I, Ingram M D and West A R 1976 *J. Electroanal. Chem.* **74** 125

[22] Doi A 1988 *Solid State Ionics* **31** 227
[23] Irvine J T S, Sinclair D C and West A R 1990 *Adv. Mater*. **2–3** 132
[24] Balzer-Jollenbeck G, Kanert O, Jain H and Ngai K L 1989 *Phys. Rev*. B **39–9** 6071
[25] Tatsumisago M, Angell C and Martin S W 1992 *J. Chem. Phys.* **97–9** 6968
[26] Elliott S R 1994 *J. Non-Cryst. Solids* **170** 97